Applied Physics Letters

Refractive index and extinction coefficient of hollow microspheres for solar reflection

Cite as: Appl. Phys. Lett. **118**, 211907 (2021); https://doi.org/10.1063/5.0049018
Submitted: 28 February 2021 • Accepted: 13 May 2021 • Published Online: 27 May 2021

Xiao Nie, Ziqi Yu, Enrique Jackson, et al.

View Online Export Citation CrossMark

ARTICLES YOU MAY BE INTERESTED IN

Reflectivity of solid and hollow microsphere composites and the effects of uniform and varying diameters
Journal of Applied Physics **128**, 053103 (2020); https://doi.org/10.1063/5.0015650

Myths and truths about optical phase change materials: A perspective
Applied Physics Letters **118**, 210501 (2021); https://doi.org/10.1063/5.0054114

Radiative sky cooling: Fundamental principles, materials, and applications
Applied Physics Reviews **6**, 021306 (2019); https://doi.org/10.1063/1.5087281

© 2021 Author(s).

Applied Physics Letters ARTICLE scitation.org/journal/apl

Refractive index and extinction coefficient of hollow microspheres for solar reflection

Cite as: Appl. Phys. Lett. **118**, 211907 (2021); doi: 10.1063/5.0049018
Submitted: 28 February 2021 · Accepted: 13 May 2021 ·
Published Online: 27 May 2021

View Online Export Citation CrossMark

Xiao Nie,[1] Ziqi Yu,[1] Enrique Jackson,[2] and Jaeho Lee[1,a)]

AFFILIATIONS

[1]Department of Mechanical and Aerospace Engineering, University of California, Irvine, California 92697, USA
[2]NASA Marshall Space Flight Center, Huntsville, Alabama 35812, USA

[a)]Author to whom correspondence should be addressed: jaeholee@uci.edu

ABSTRACT

While hollow microspheres and various porous structures have received much attention for solar reflection in the recent literature, their fundamental determinants of optical properties and material selection criteria are relatively little known. Here, we study hollow microspheres with varying refractive index and extinction coefficient and identify their role in determining the solar reflectivity. Our simulations based on finite-difference time-domain method show the effects of refractive index between 1.5 and 100 and extinction coefficient between 10^{-6}–10^{0} in the wavelength region of 0.2–2.4 μm and explain how the reflectivity of hollow microspheres is attributed to a combination of strong back-scattering and limited absorption. Our analysis indicates that ceramic materials with a high refractive index and a low extinction coefficient such as Y_2O_3 are promising. When Y_2O_3 hollow microspheres are randomly distributed with the diameter ranging from 0.5 to 1 μm, our simulation shows the solar reflectivity reaches 0.97 even at 300 μm thickness, and a diffusion theory-based model predicts the solar reflectivity to exceed 0.98 at 500 μm or 0.99 at 1 mm thickness. Our findings can guide optimal designs of hollow microspheres and related porous structures toward complete solar reflection and enable breakthroughs in thermal management and deep-space applications.

© 2021 Author(s). All article content, except where otherwise noted, is licensed under a Creative Commons Attribution (CC BY) license (http://creativecommons.org/licenses/by/4.0/). https://doi.org/10.1063/5.0049018

Considering the large amount of solar irradiance an object in space receives, a wide variety of thermal control coatings were developed to aid in thermal managements of spacecraft. Optical coatings that reflect sunlight in the wavelengths of 0.2–2.4 μm, which cover the ultraviolet, visible, and near-infrared regions, may lead to significant surface cooling and energy savings for buildings,[1–3] spacecraft thermal control in extreme environments,[4,5] and efficient heliostats for concentrating solar power plants.[6,7]

Over the past decades, several experimental and numerical demonstrations of perfect reflection have been reported[8–10] using all-dielectric metamaterials. However, narrow bandwidth limits its application in shielding high-power irradiation such as solar irradiation. Metallic reflectors[5,11] and distributed Bragg reflectors[12–14] are commonly used to achieve broadband high solar reflectivity. However, metallic reflectors cannot provide high solar reflectivity in the wavelength region of 0.3–0.5 μm, and Bragg reflectors composed of alternating layers are typically made by sophisticated fabrication techniques, which require either many layers or expensive metallic films to achieve the desired reflectivity.

Another inexpensive and scalable solution for achieving broadband near-perfect solar reflectivity is to fabricate dielectric nanoparticle-polymer composites[1,15–18] using hierarchical porous polymer[17,18] or hollow microspheres.[1,16,19,20] Hollow microspheres made of dielectric materials[1,16,20] or polymers[19] are studied to exhibit broadband high solar reflectivity. For instance, our previous work[1,20] shows that hollow microsphere designs enable low-refractive-index materials, such as SiO_2, to have higher backscattering intensity compared to solid microspheres.

In addition to novel solar reflector discovery, analytical and numerical studies[20,21] based on Mie theory, Monte Carlo method, and finite-difference time-domain (FDTD) method have been performed to investigate mechanism for high solar reflectivity. Our recent study[20] based on two-dimensional (2D) FDTD method indicates that hollow microspheres with a thin shell induce stronger scattering and lead to a higher solar reflectivity. Despite these efforts, little attention has been paid to material selection principles for solar reflectivity enhancement. In this work, we conduct a systematic study on composite systems using randomly distributed hollow microspheres from 0.5 μm to 1 μm

© Author(s) 2021

based on 2D FDTD computations. We separately investigate the effects of refractive index and extinction coefficient in hollow microsphere on weighted solar reflectivity in the solar wavelength region of 0.2–2.4 μm. We also identify several materials that lead to broadband ultrahigh solar reflectivity with a small thickness. These findings could help to benefit solar reflector designs.

Our previous work[20] has demonstrated that hollow microspheres enable low-refractive-index materials (such as SiO_2) to exhibit high solar reflectivity, and they indicate an enhanced solar reflectivity when hollow SiO_2 microspheres are replaced with hollow TiO_2 microspheres. In the solar region, TiO_2 has a refractive index of ~2.5, which is higher than the refractive index of SiO_2 (~1.45). The refractive index difference between two materials, along with the fact that high-refractive-index materials are commonly used in solar reflective materials, motivates us to study the effect of refractive index in improving solar reflectivity. Previous studies[22,23] proposed various effective medium approximations to predict the dielectric and optical properties of composite systems by treating them as homogeneous media with effective refractive index and extinction coefficient values denoted by n_{eff} and k_{eff}, respectively. At normal incidence, Fresnel reflectivity[24] on the interface of the composite film can be simplified as $R = \left((n_{eff} - n_1)/(n_{eff} + n_1)\right)^2$, where n_1 is the medium from which the irradiance comes. Larger n_{eff} is expected when hollow microspheres with higher-refractive-index materials are dispersed in the composite system, which leads to increasing R. Effective medium approximations based on series,[25] parallel,[26] three-dimensional (3D) Maxwell–Garnett theory (MGT)[22] and volume-averaging theory (VAT)[27,28] are considered to provide an analytical approach to the reflectivity of the SiO_2 hollow microsphere composites (Fig. S1). Among them, The VAT model predicts the highest reflectivity, and the relationship between the effective reflectivity and the refractive index of hollow microspheres is presented in Fig. 1(b). VAT models can be expressed as

$$n_{eff}^2 = \frac{1}{2}\left[A + \sqrt{A^2 + B^2}\right], \tag{1}$$

$$A = \varepsilon_{r,eff} = \phi\left(n_d^2 - k_d^2\right) + (1-\phi)\left(n_c^2 - k_c^2\right), \tag{2}$$

$$B = 2n_d k_d \phi + 2n_c k_c (1-\phi), \tag{3}$$

where n and k, respectively, refer to the refractive index and extinction coefficient of the continuous medium (subscript c) and the dispersed medium (subscript d), and ϕ is the volume fraction of the dispersed medium.

While the analytical models based on the effective medium approximations capture the trend of increasing R with increasing n_{eff}, they do not account for the Mie scattering effect,[29] which is important for hollow microspheres whose dimensions are comparable to the wavelength of interest. For that reason, the VAT model may underpredict the reflectivity of hollow microsphere composites, and to account for the Mie scattering effect, numerical simulations based on the

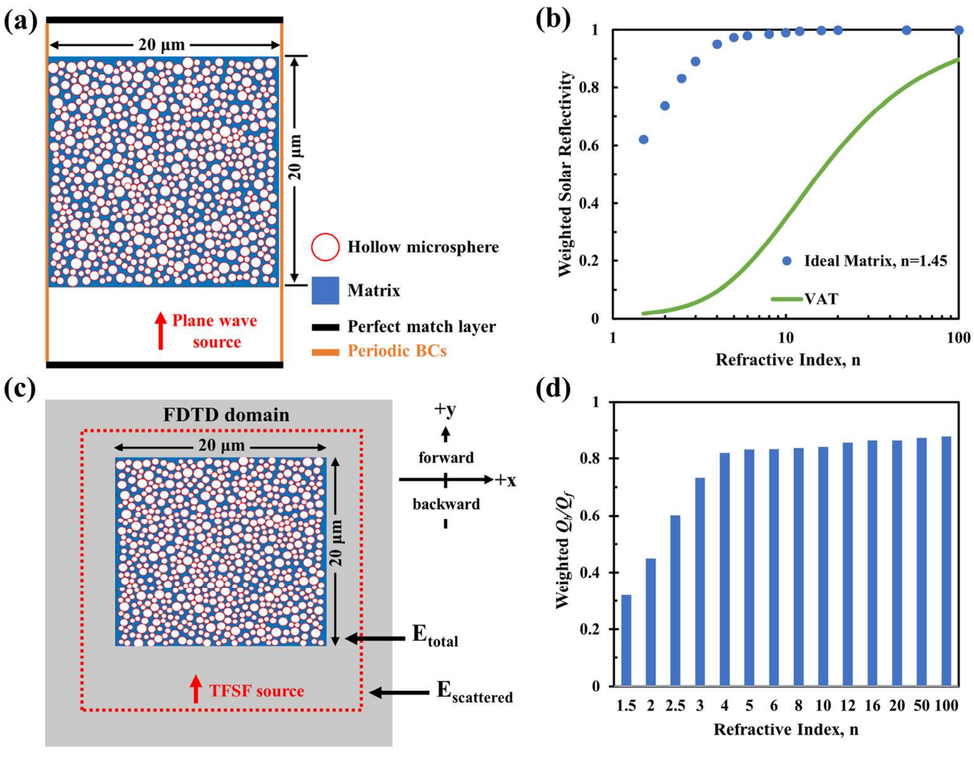

FIG. 1. The effect of refractive index (n) in hollow microspheres. (a) The schematic of 2D FDTD unit cell; (b) $R_{weighted}$ from 0.2–2.4 μm for different n from 1.5 to 100 in hollow microspheres using the ideal matrix material (n = 1.45, k = 0). The analytical results using the VAT model and simplified Fresnel reflectivity is also plotted (green); (c) the schematic of the 2D unit cell with total-field-scatter-field (TFSF) wave source; (d) Spectrally average backscattering ratio Q_b/Q_f of different n in hollow microspheres.

© Author(s) 2021

FDTD method are used in this work. FDTD is the method providing solutions to Maxwell's equations in a discretized unit cell. We set a unit cell with a dimension of 20 μm $\times$ 20 μm in 2D FDTD domain [Fig. 1(a)]. We choose to work with 2D instead of 3D unit cells since changing the dimensionality of the simulation does not change the results as the hollow microspheres are symmetric in both 2D and 3D. The fact that 3D simulations are much more computationally expensive compared to 2D is another reason we choose to work with 2D (see supplementary material for details). Inside the unit cell, we generated the closely packed random hollow microspheres with a diameter range of 0.5–1 μm and an inner-to-outer diameter ratio d_i/d_o of 0.9,[20] which gives a final areal fraction of 58.56%. The areal fraction is the fraction of total areas of 2D microspheres over the area of the unit cell and it can be calculated as $Areal\,Fraction = \sum_{i=1}^{N} \pi r_i^2/(20 \times 20)$, where r_i is the radius of ith circle with a unit of μm and N is the total number of microspheres. To evaluate the effect of refractive index (n) in hollow microspheres on solar reflectivity, we set n to wavelength-independent values from 1.5 to 100, while keeping the extinction coefficient as 0. It should be noted that the range of refractive index from 1.5 to 100 may not be realistic or experimentally accessible, but this study explores this range in computations to show the potential impact of very high refractive index on reflectivity and provide a general understanding of optical properties of hollow microspheres. We utilize an ideal matrix material by setting the refractive index as 1.45 and extinction coefficient as 0 to eliminate any absorption from the matrix. The matrix is a binding material that can be a polymer such as PDMS.

We calculated the weighted solar reflectivity ($R_{weighted}$) using the spectral reflectivity based on solar spectrum distribution,[13]

$$R_{weighted} = \frac{\int_{0.2}^{2.4} R(\lambda) I_{AM1.5}(\lambda)\, d\lambda}{\int_{0.2}^{2.4} I_{AM1.5}(\lambda)\, d\lambda}, \tag{4}$$

where $I_{AM1.5}(\lambda)$ is the solar irradiance with an air mass of 1.5. When we set n value to 1.5, $R_{weighted}$ is 0.6215 for the ideal matrix whose $n = 1.45$. It is evident from Fig. S2 and Fig. 1(b) that $R_{weighted}$ increases with increasing n and the increment becomes asymptotically smaller with n approaching 100. The solar reflectivity is reduced slightly when PDMS is used as the matrix material [Fig. S2(c)] because of its non-zero k values in the solar region.[30] In Fig. 1(b), we show the analytical results calculated using n_{eff} calculated from VAT[27,28] and simplified Fresnel reflectivity equation at normal incidence assuming n_1 equals to 1 as a comparison. The difference between FDTD results and VAT calculations can be explained by the fact that effective medium approximations[31,32] do not effectively take into account the Mie scattering efficiency[29] of hollow microspheres in the composite system.[33] The enhancement of $R_{weighted}$ is further evidenced in FDTD computations using a total-field-scatter-field (TFSF) source [Fig. 1(c)], which is generally used to capture the scattering efficiency of the structure.[34,35] The unit cell and distribution of hollow microspheres inside remains the same so that the areal fraction of hollow microspheres keeps 58.56%. The forward scattering efficiency (Q_f) and the backward scattering efficiency (Q_b) are both simulated, and we use a backward-to-forward scattering ratio Q_b/Q_f to represent the capability of the structure to backscatter incident irradiance. As shown in Fig. 1(d), spectrally integrated Q_b/Q_f increases from 0.3202 to 0.8783 as n increases from 1.5 to 100, which agrees with $R_{weighted}$ enhancement in FDTD computations using a plane wave source.

After understanding the effect of n values in solar reflectivity, we investigate the effect of extinction coefficients (k) with the same model. For each n, we vary k values from 10^{-6} to 10^{0}. Figure 2(a) and S3(a) shows the effect of k values while $n = 1.5$. When we set k value as 10^{0}, $R_{weighted}$ is only 0.0559 in the solar region of 0.2–2.4 μm. Decreasing k value from 10^{0} to 10^{-4} leads to increased $R_{weighted}$ from 0.0559 to 0.5908. It is also noticed that $R_{weighted}$ remains almost unchanged when k changes from 10^{-4} to 10^{-6}. The increase in $R_{weighted}$ is only 0.62%. We further calculate the spectral absorptivity $\varepsilon(\lambda)$ = 1-R(λ)−T(λ) and weighted solar absorptivity ($\varepsilon_{weighted}$) values based on the solar spectrum distribution

$$\varepsilon_{weighted} = \frac{\int_{0.2}^{2.4} \varepsilon(\lambda) I_{AM1.5}(\lambda)\, d\lambda}{\int_{0.2}^{2.4} I_{AM1.5}(\lambda)\, d\lambda}. \tag{5}$$

It is evident from Fig. S3(b) that $\varepsilon_{weighted}$ in the solar region decreases with decreasing k from 10^{0} to 10^{-6} and approaches 0 when k is equal to or smaller than 10^{-4}, when n equals to 1.5.

The similar trend is observed as well when n value is increased and k value is varied. Using n values ranging from 1.5 to 100 and k

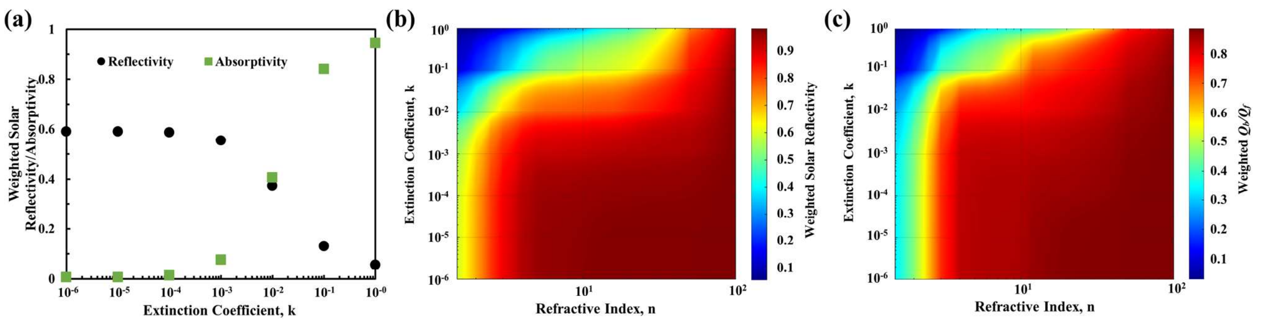

FIG. 2. The effect of extinction coefficient (k) in hollow microspheres. (a) $R_{weighted}$ and $\varepsilon_{weighted}$ in 0.2–2.4 μm for different k from 10^{-6} to 10^{0} in hollow microspheres, with the refractive index (n) setting to 1.5; (b) $R_{weighted}$ and (c) weighted Q_b/Q_f in 0.2–2.4 μm as a function of various n and k values in hollow microspheres. Color legends are used to represent $R_{weighted}$ and weighted Q_b/Q_f values.

© Author(s) 2021

values ranging from 10^{-6} to 10^{0}, $R_{weighted}$ can be plotted as a function of both values, as shown in Fig. 2(b). It is noticed that when n is as large as 20 or more, $R_{weighted}$ at extinction coefficient equals to 1 is more than 0.8 and the solar reflectivity increment with decreasing k is much smaller compared to the increment at $n = 1.5$. This phenomenon can also be found when we evaluate the backward-to-forward scattering ratio Q_b/Q_f using the TFSF source in the simulations [Fig. 2(c)]. We believe the plots could provide the material selection guidance for a combination of two components in optical constants to achieve desired solar reflectivity, which could be used to perfect solar reflectivity optimization.

The investigations on the effect of n and k values indicate that materials with a high n and low k in the solar region are preferred for a high solar reflectivity in such hierarchical hollow-microsphere-embedded polymeric systems. We have previously demonstrated high solar reflectivity by integrating SiO_2 hollow microspheres within PDMS,[1,20] and we would like to find out some other material candidates that could also be promising to achieve high solar reflectivity. Here, several ceramic materials are chosen since they exhibit similar optical constants as SiO_2. Figures 3(a) and 3(b) shows n and k values of SiO_2, TiO_2, yttrium oxide (Y_2O_3), magnesium fluoride (MgF_2), cerium trifluoride (CeF_3), and strontium fluoride (SrF_2). All the optical constants are obtained from previous publications,[36–39] and optical constants of MgF_2 and CeF_3 are only from wavelength of 0.2 μm to 2 μm according to previous work.[38] It is found that TiO_2 has the highest n value in the solar region and a very high k value in the ultraviolet region. When we use these optical constants as the input for our 2D FDTD computations while using the ideal matrix material [Fig. 3(c)], we can compare the solar reflectivity spectrum in Fig. 3(d) and average reflectivity values in three separate regions in the solar wavelength region in Table I. The solar wavelength of 0.2–2.4 μm can be divided into three separate regions:[13] ultraviolet (UV) region in 0.2–0.4 μm, visible region in 0.4–0.8 μm, and near-infrared (NIR) region in 0.8–2.4 μm. Our simulations indicate that with a thickness of 20 μm, Y_2O_3 hollow microsphere contributes to the highest $R_{weighted}$ of 0.7154, due to its high n and low k value throughout the solar region. Because of 6% solar irradiation intensity in the UV region, $R_{weighted}$ of Y_2O_3 is higher than that of TiO_2 ($R_{weighted} = 0.7076$). The comparison between SiO_2 or Y_2O_3 hollow-microsphere-based composite using PDMS as the matrix material with porous PDMS (Fig. S4) indicates that hollow microspheres more effectively achieve higher solar reflectivity than hierarchical porous polymer. Compared to previously reported SiO_2 hollow microspheres, Y_2O_3 hollow microspheres exemplify its potential application in perfect solar reflectors.

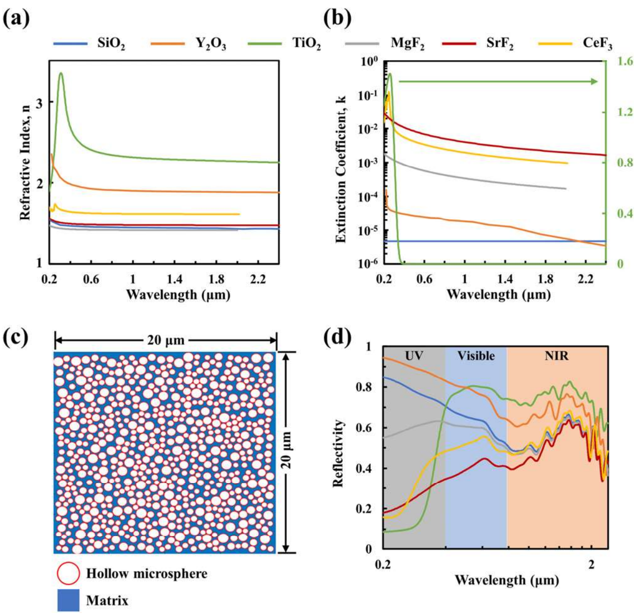

FIG. 3. The solar reflectivity of hollow-microspheres-embedded composites with naturally existing or commonly used ceramic pigment materials. (a) n and (b) k values from 0.2–2.4 μm for various pigment materials. The extinction coefficient curve of TiO_2 corresponds to y-axis in the right, while other curves correspond to the y-axis on the left; (c) the schematic of the composite system in FDTD simulations; and (d) the solar reflectivity spectrum in the solar region of 0.2–2.4 μm for different materials.

The simulation result indicates the potential of Y_2O_3 hollow microspheres for broadband near-perfect solar reflectors, which achieves a $R_{weighted}$ of 0.7154 with a thickness of 20 μm. We thus study the thickness dependence of Y_2O_3 hollow-microsphere-based composite systems. We set the thickness to 20, 50, 100, and 300 μm [Fig. 4(a)], which are some general thicknesses used for coatings,[15–17] while maintaining the areal fraction as 58.56%. It shows that with a higher thickness of 50, 100, and 300 μm, $R_{weighted}$ is enhanced to 0.8504, 0.9226, and 0.9664, respectively [Fig. 4(b)]. Besides FDTD simulations, we also study the thickness dependence using the diffusion theory[17,40–43] involving transport mean free path (l^*), which is the length over which the direction of propagation of the photon is randomized. The diffusion theory relates transmissivity of the composite system (T) to its thickness (L) by the following equation:[31,42,43]

$$T = \frac{l^*(1+s)}{L + 2l^* s}. \quad (6)$$

In Eq. (6), s is the extrapolation length ratio that can be calculated using $s = 2(1+R)/[3(1-R)]$, where R is the internal reflectance. VAT[27,28] and 3D MGT[22] models are used to estimate the value of s by using the refractive index of Y_2O_3 ($n = 1.9$) and PDMS ($n = 1.45$), and the areal fraction of 58.56%. We use the spectrally independent refractive index values in the calculation for the convenience. The spectral reflectivity (R_s) is calculated using $R_s = 1 - T$. Figure 4(c) indicates the thickness dependence on solar reflectivity of Y_2O_3

TABLE I. Averaged reflectivity for various pigment materials in three different wavelength regions: UV, visible, and NIR region. $R_{weighted}$ is calculated using Eq. (4).

Materials	UV (0.2–0.4 μm)	Visible (0.4–0.8 μm)	NIR (0.8–2.4 μm)	$R_{weighted}$
SiO_2	0.7770	0.6096	0.5360	0.5873
TiO_2	0.2489	0.7589	0.7288	0.7076
Y_2O_3	0.8888	0.7401	0.6643	0.7154
MgF_2	0.6054	0.5720	0.5253	0.5525
SrF_2	0.2652	0.4080	0.5066	0.4438
CeF_3	0.3299	0.5133	0.5514	0.5178

© Author(s) 2021

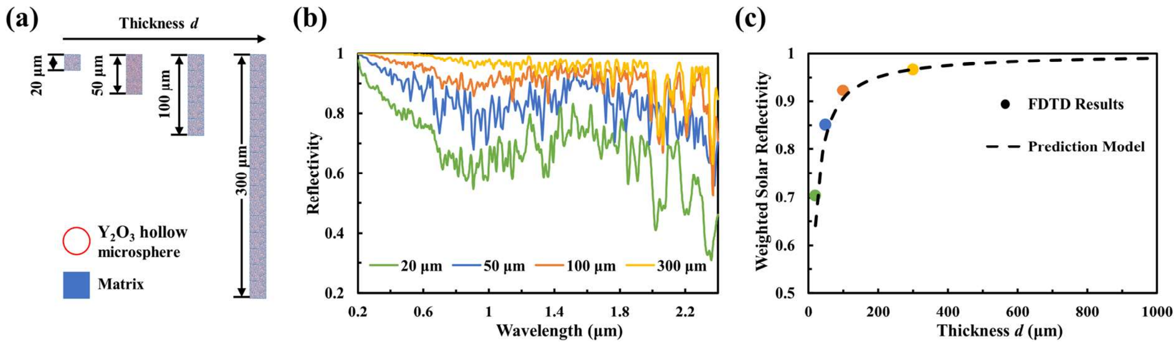

FIG. 4. Thickness-dependent solar reflectivity of Y_2O_3 hollow-microsphere-based composites. (a) The schematic of Y_2O_3 hollow-microsphere-based composites with a thickness of 20, 50, 100, and 300 μm. The parameter $\boldsymbol{d}$ is the thickness of the composite; (b) the solar reflectivity spectrum with a thickness of 20, 50, 100, and 300 μm; (c) $R_{weighted}$ as a function of thickness and reflectivity predictions based on the diffusion theory for a thickness of 20–1000 μm. $R_{weighted}$ is calculated using Eq. (4) and the prediction uses the VAT model defined in Eqs. (1)–(3) and the diffusion theory in Eq. (6).

hollow-microsphere-based composites with an ideal matrix material from a thickness of 20 μm to 1000 μm using the diffusion theory, which shows the agreement with the FDTD simulation results with a thickness of 20 μm, 50 μm, 100 μm, and 300 μm. Both MGT and VAT approximations show the identical predictions (Fig. S5), which indicate a solar reflectivity beyond 0.98 for a thickness of larger than 500 μm. The solar reflectivity we demonstrate is among the highest solar reflectivity for such polymeric systems with similar thicknesses (Table II) and we believe Y_2O_3 hollow microspheres is promising to achieve near-perfect solar reflectivity which benefits applications for spacecraft, buildings, or electronics.

To sum up, we investigate the effects of refractive index and extinction coefficient values on solar reflectivity in randomly distributed hierarchical hollow microsphere with a diameter range of 0.5–1 μm and an inner-to-outer diameter ratio d_i/d_o of 0.9 using FDTD simulations. The weighted solar reflectivity ($R_{weighted}$) in the wavelength region of 0.2–2.4 μm increases from 0.5902 to 0.9913 as the refractive index increases from 1.5 to 100 due to enhanced backscattering, which is supported by the increasing value of backward-to-forward scattering ratio Q_b/Q_f. We also demonstrate that the solar reflectivity enlarges with a smaller extinction coefficient because of weaker solar absorption. By implementing with various refractive index values from 1.5 to 100 and extinction coefficient values from 10^{-6} to 10^{0} we obtain the contour plots showing $R_{weighted}$ and Q_b/Q_f variations, which provide the guideline for material selections for broadband perfect solar reflectivity. Our study indicates ceramic materials with the combination of high refractive index and low extinction coefficient values such ,as Y_2O_3 are promising candidates. Our FDTD simulation indicates a $R_{weighted}$ of 0.9664 with a 300 μm thickness with Y_2O_3 hollow microspheres. In addition, the diffusion theory we utilize in Y_2O_3 hollow-microspheres-based composite indicates a $R_{weighted}$ of 0.98 at a 500-μm thickness and 0.99 at a 1-mm thickness. This work helps to identify the desired optical constants to achieve a broadband perfect solar reflectivity and provides a material selection guidance for

TABLE II. State-of-the-art polymeric systems with high solar reflectivity in previous publications.[15,17,21,43–45]

Materials	Experiment/simulation	Thickness	Weighted solar reflectivity	References
Randomly packed SiO_2 microsphere	Experiment	700 μm	0.9926	43
6% SiO_2+TPX matrix + 200 nm Ag	Experiment	50 μm	0.9517	15
Hierarchical porous PVDF-HFP	Experiment	100 μm	0.86	17
		150 μm	0.875	
		200 μm	0.9	
		300 μm	0.96	
		480 μm	0.98	
TiO_2 nanoparticles+ resin	Experiment	2 mm	0.87	21
	Simulation	1 mm	0.91	
$CaCO_3$+resin	Experiment	98 μm	0.889	44
		131 μm	0.934	
		177 μm	0.951	
		400 μm	0.955	
TiO_2+hollow thermoplastic microspheres	Experiment	600 μm	0.8546	45

© Author(s) 2021

pigment-embedded polymeric materials. We believe this work provides the findings that can be potentially utilized to optimize solar reflectivity or radiative cooling performance for the deep-space and building applications.

See the supplementary material for more details about the effective medium approximations, 2D FDTD simulations, and the comparison between 2D and 3D FDTD simulations.

J.L., X.N., and Z.Y. thank the support provided by NASA MSFC through Cooperative Agreement No. 80NSSC20M0180 and by the National Science Foundation (No. ECCS-1935843).

DATA AVAILABILITY

The data that support the findings of this study are available from the corresponding author upon reasonable request.

REFERENCES

[1]X. Nie, Y. Yoo, H. Hewakuruppu, J. Sullivan, A. Krishna, and J. Lee, Sci. Rep. **10**, 1–10 (2020).

[2]T. Li, Y. Zhai, S. He, W. Gan, Z. Wei, M. Heidarinejad, D. Dalgo, R. Mi, X. Zhao, J. Song, J. Dai, C. Chen, A. Aili, A. Vellore, A. Martini, R. Yang, J. Srebric, X. Yin, and L. Hu, Science **364**, 760 (2019).

[3]X. Li, B. Sun, C. Sui, A. Nandi, H. Fang, Y. Peng, G. Tan, and P. C. Hsu, Nat. Commun. **11**, 1–9 (2020).

[4]R. C. Youngquist, M. A. Nurge, W. L. Johnson, T. L. Gibson, and J. M. Surma, J. Spacecr. Rockets **55**, 622 (2018).

[5]K. N. Marshall and R. A. Breuch, J. Spacecr. Rockets **5**, 1051 (1968).

[6]A. Fernández-García, M. E. Cantos-Soto, M. Röger, C. Wieckert, C. Hutter, and L. Martínez-Arcos, Sol. Energy Mater. Sol. Cells **130**, 51 (2014).

[7]D. Barlev, R. Vidu, and P. Stroeve, Sol. Energy Mater. Sol. Cells **95**, 2703 (2011).

[8]B. Slovick, Z. G. Yu, M. Berding, and S. Krishnamurthy, Phys. Rev. B **88**, 165116 (2013).

[9]P. Moitra, B. A. Slovick, Z. Gang Yu, S. Krishnamurthy, and J. Valentine, Appl. Phys. Lett. **104**, 171102 (2014).

[10]P. Moitra, B. A. Slovick, W. Li, I. I. Kravchencko, D. P. Briggs, S. Krishnamurthy, and J. Valentine, ACS Photonics **2**, 692 (2015).

[11]J. long Kou, Z. Jurado, Z. Chen, S. Fan, and A. J. Minnich, ACS Photonics **4**, 626 (2017).

[12]M. Santamouris and J. Feng, Building **8**, 168 (2018).

[13]M. M. Hossain and M. Gu, Adv. Sci. **3**, 1500360 (2016).

[14]A. P. Raman, M. A. Anoma, L. Zhu, E. Rephaeli, and S. Fan, Nature **515**, 540 (2014).

[15]Y. Zhai, Y. Zhai, Y. Ma, S. N. David, D. Zhao, R. Lou, G. Tan, R. Yang, and X. Yin, Science **355**, 1062 (2017).

[16]Z. Xing, S. W. Tay, Y. H. Ng, and L. Hong, ACS Appl. Mater. Interfaces **9**, 15103 (2017).

[17]J. Mandal, Y. Fu, A. Overvig, M. Jia, K. Sun, N. Shi, H. Zhou, X. Xiao, N. Yu, and Y. Yang, Science **362**, 315 (2018).

[18]D. Li, X. Liu, W. Li, Z. Lin, B. Zhu, Z. Li, J. Li, B. Li, S. Fan, J. Xie, and J. Zhu, Nat. Nanotechnol. **16**, 153–158 (2020).

[19]J. D. Alden, S. Atiganyanun, R. Vanderburg, S. H. Lee, J. B. Plumley, O. K. Abudayyeh, S. M. Han, and S. E. Han, J. Photonics Energy **9**, 1 (2019).

[20]Z. Yu, X. Nie, A. Yuksel, and J. Lee, J. Appl. Phys. **128**, 053103 (2020).

[21]J. Peoples, X. Li, Y. Lv, J. Qiu, Z. Huang, and X. Ruan, Int. J. Heat Mass Transfer **131**, 487 (2019).

[22]J. C. M. Garnett and J. Larmor, Proc. R. Soc. London **203**, 359–371 (1904).

[23]N. J. Hutchinson, T. Coquil, A. Navid, and L. Pilon, Thin Solid Films **518**, 2141 (2010).

[24]D. B. Judd, J. Res. Natl. Bur. Stand. **29**, 329 (1942).

[25]M. M. Braun and L. Pilon, Thin Solid Films **496**, 505 (2006).

[26]A. Sihvola, *Electromagnetic Mixing Formulas Application* (IET, 1999).

[27]J. A. Del Río and S. Whitaker, Transp. Porous Media **39**, 159 (2000).

[28]J. A. Del Río and S. Whitaker, Transp. Porous Media **39**, 259 (2000).

[29]C. F. Bohren, *Absorption Scattering Light by Small Particles* (John Wiley & Sons, 1983).

[30]M. Querry, *Optical Constants of Minerals and Other Materials From the Millimeter to the Ultraviolet* (Chemical Research, Development & Engineering Center, US Army Armament Munitions Chemical Command, 1987).

[31]L. Schertel, L. Siedentop, J. M. Meijer, P. Keim, C. M. Aegerter, G. J. Aubry, and G. Maret, Adv. Opt. Mater. **7**, 1900442 (2019).

[32]L. Schertel, I. Wimmer, P. Besirske, C. M. Aegerter, G. Maret, S. Polarz, and G. J. Aubry, Phys. Rev. Mater. **3**, 015203 (2019).

[33]V. Demontis, A. Marini, F. Floris, L. Sorba, and F. Rossella, AIP Conf. Proc. **2257**, 020009 (2020).

[34]S. Tanev, V. Tuchin, P. Cheben, P. Bock, J. Schmid, S. Janz, D. Xu, J. Lapointe, A. Densmore, and J. Pond, Photonic Nanostruct. **9**, 315–327 (2011).

[35]S. Tanev, V. V. Tuchin, and P. Paddon, Laser Phys. Lett. **3**, 594 (2006).

[36]T. Siefke, S. Kroker, K. Pfeiffer, O. Puffky, K. Dietrich, D. Franta, I. Ohlídal, A. Szeghalmi, E. B. Kley, and A. Tünnermann, Adv. Opt. Mater. **4**, 1780 (2016).

[37]Y. Nigara, Jpn. J. Appl. Phys., Part 1 **7**, 404 (1968).

[38]L. V. Rodríguez-de Marcos, J. I. Larruquert, J. A. Méndez, and J. A. Aznárez, Opt. Mater. Express **7**, 989 (2017).

[39]L. R. De Marcos, J. I. Larruquert, J. A. Aznárez, M. Fernández-Perea, R. Soufli, J. A. Méndez, S. L. Baker, and E. M. Gullikson, J. Appl. Phys. **113**, 143501 (2013).

[40]M. U. Vera and D. J. Durian, Phys. Rev. E **53**, 3215 (1996).

[41]P. D. Kaplan, A. D. Dinsmore, A. G. Yodh, and D. J. Pine, Phys. Rev. E **50**, 4827 (1994).

[42]F. Y. De Boer, R. J. A. Van Dijk-Moes, A. Imhof, and K. P. Velikov, Langmuir **35**, 12091 (2019).

[43]S. Atiganyanun, J. B. Plumley, S. J. Han, K. Hsu, J. Cytrynbaum, T. L. Peng, S. M. Han, and S. E. Han, ACS Photonics **5**, 1181 (2018).

[44]X. Li, J. Peoples, Z. Huang, Z. Zhao, J. Qiu, and X. Ruan, arXiv (2020).

[45]O. Sandin, J. Nordin, and M. Jonsson, J. Coat. Technol. Res. **14**, 817 (2017).

© Author(s) 2021